Electronic Supplementary Information (ESI) for:

Mechanisms of interaction between bismuth-based materials and contaminants for subsurface remediation

*Carolyn I. Pearce [*a] , Daria Boglaienko[*a], Amanda R. Lawter[a], Elsa A. Cordova[a], Kirk J. Cantrell[a], Mark E. Bowden[a], Nabajit Lahiri[a], Odeta Qafoku [a], Sebastian T. Mergelsberg[a], Charles T. Resch[a], Ferdinan Cintron Colon [a], Vanessa A. Garayburu-Caruso[a], Nicolas D'Annunzio[a], Mahalingam Balasubramanian[b], Sarah A. Saslow[a], Nikolla P. Qafoku[a], Vicky L. Freedman[a], Tatiana G. Levitskaia [*a]*

[a]Pacific Northwest National Laboratory (PNNL), 902 Battelle Boulevard, Richland, WA 99352

[b]Advanced Photon Source, Argonne IL 60439

*Author to whom correspondence should be addressed.

Address: Pacific Northwest National Laboratory (PNNL), P.O. Box 999, Richland, WA 99352

For submission to Journal of Materials Chemistry A

Summary of Supporting Information: 17 pages (including cover page), 21 Figures, 5 Tables

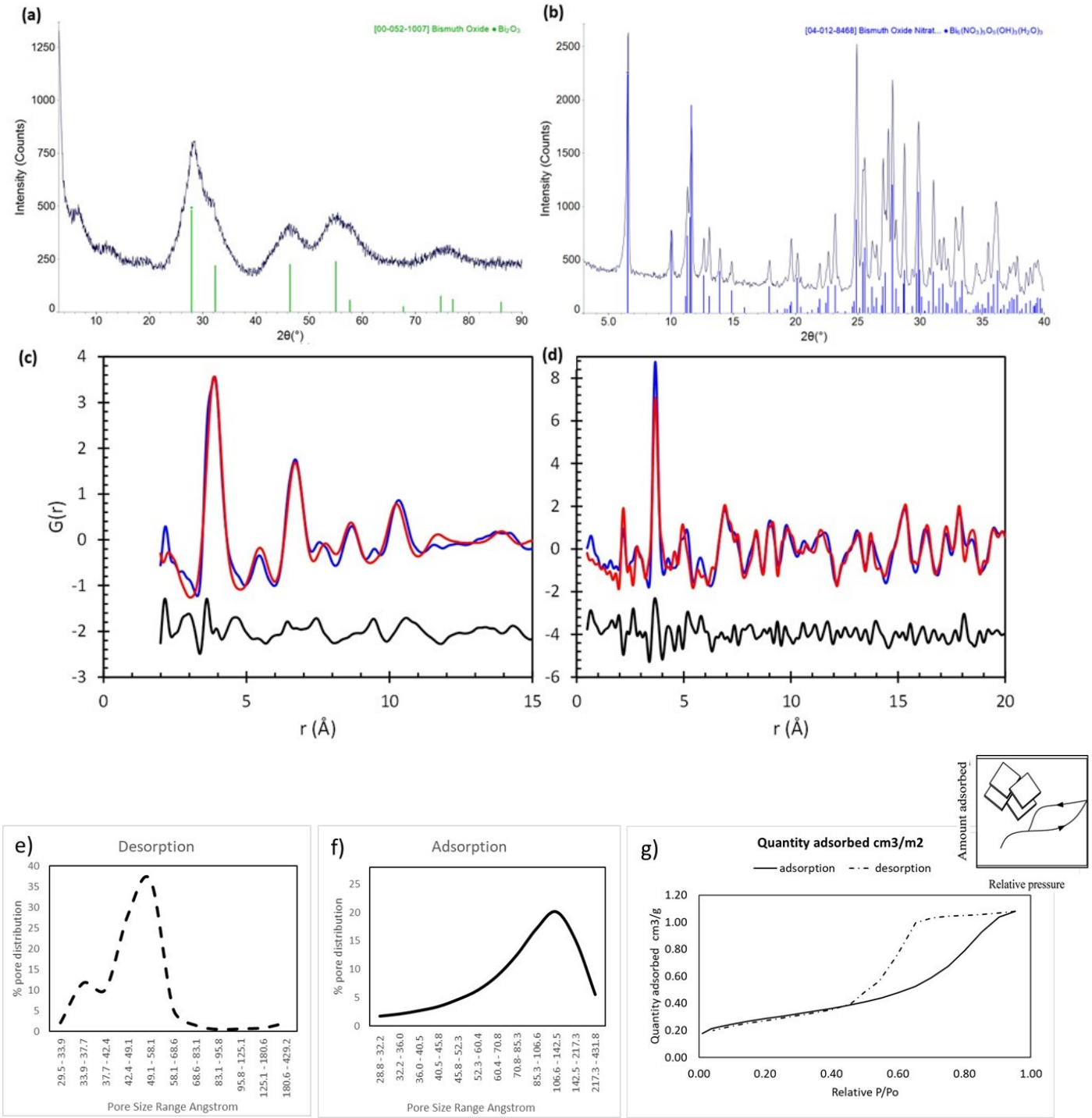

Figure S1: XRD pattern for (a) BOH overlaid with the pattern for a bismuth oxide (Bi_2O_3) and (b) for BSN overlaid with the pattern for bismuth basic nitrate $[Bi_6O_5(OH)_3]^{5+}$ clusters from Lazarini et al. 1978. Rietveld-type refinement of XPDF data (data shown in blue, fit shown in red and residual shown in black) for: (c) BOH material and (d) BSN material. BOH desorption calculated curve for pore size distribution (incremental pore volume/cumulative pore volume) relative to the pore size range (e), adsorption calculated curve for pore size distribution (incremental pore volume/cumulative pore volume) relative to the pore size range (f), and adsorption isotherm (shape of pores is shown in inset from Zhen et al., 2017) (g).

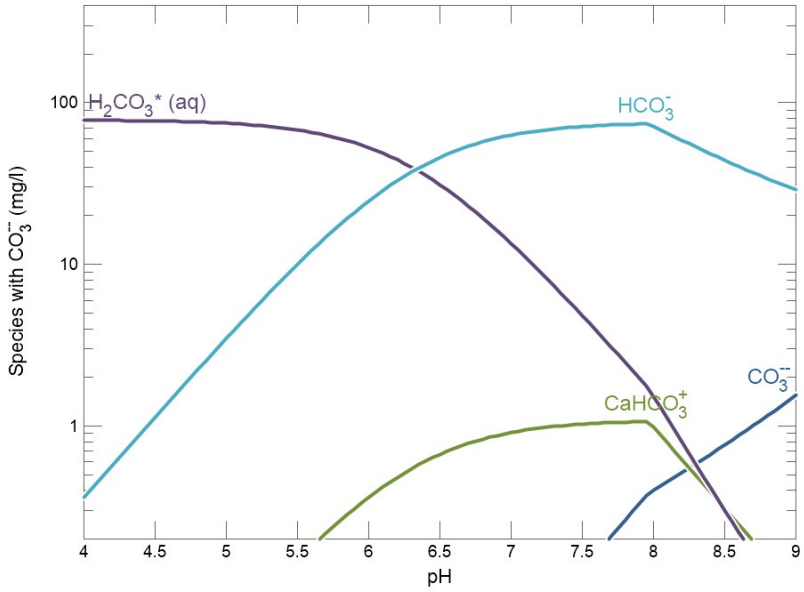

Figure S2: Speciation diagram for carbonate species in Hanford SGW depending on pH. The actual concentrations may not be exact for the system open to the atmosphere. H_2CO_3* = CO_2(aq) + H_2CO_3, where CO_2(aq) >> H_2CO_3.

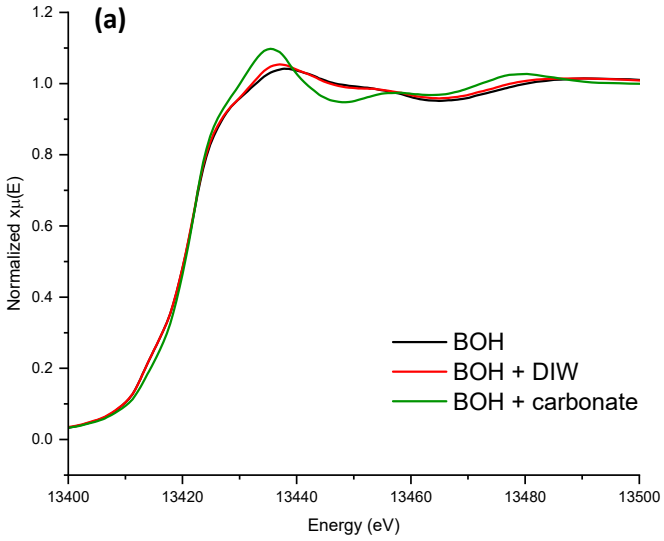

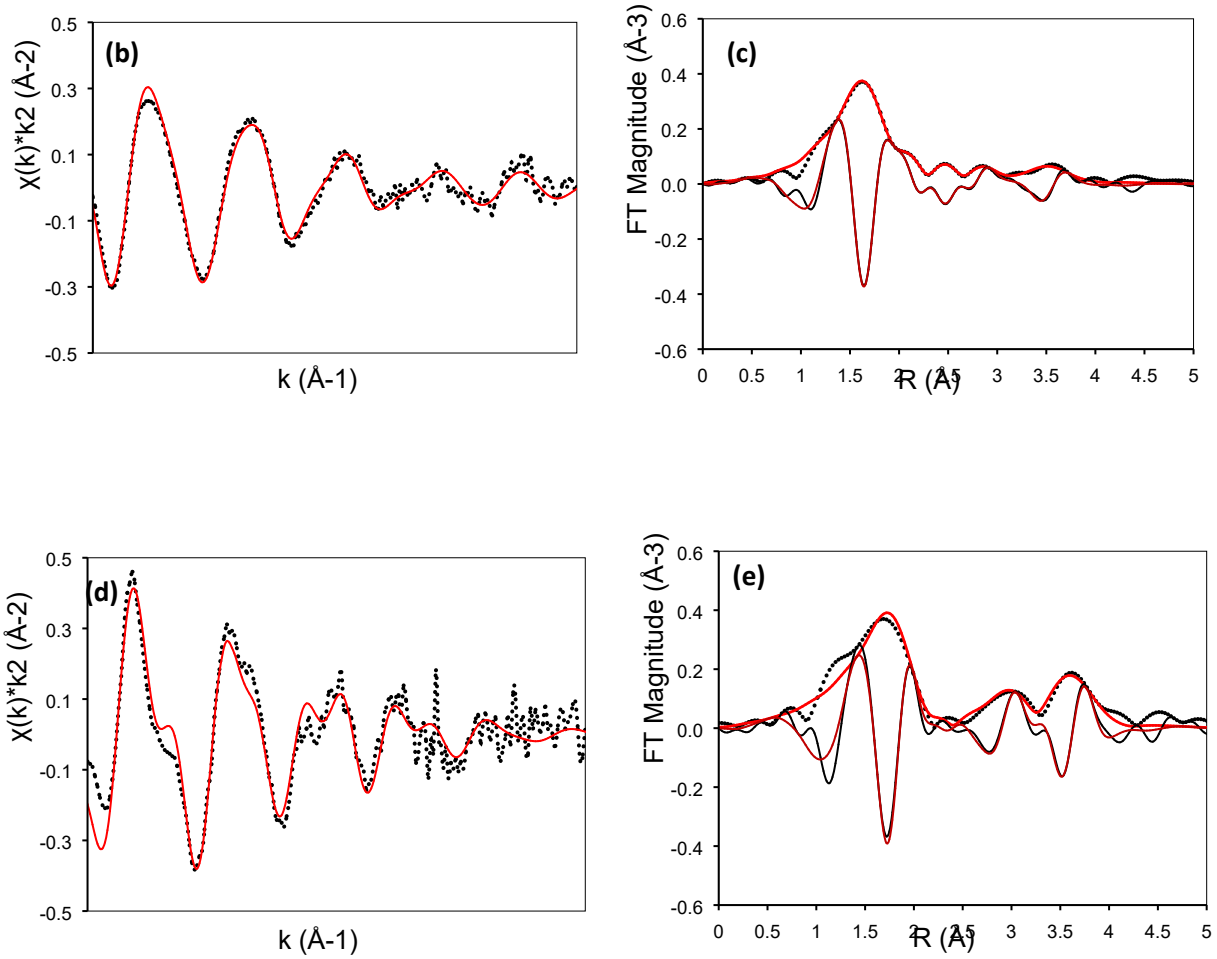

Figure S3: Bi L_{III}-edge XAS for BOH exposed to DIW and BOH exposed to carbonate. (a) XANES for BOH exposed to DIW and carbonate. (b) EXAFS and (c) transform magnitude with imaginary part for BOH exposed to DIW. (d) EXAFS and (e) transform magnitude with imaginary part for BOH exposed to carbonate. Black lines are data and solid red lines are fit. Fit with k-range 3-12.5 $Å^{-1}$ and R-range: 1.2-4.2 Å.

Table S1. EXAFS fit to Bi L_{III}-edge data for BOH exposed to DIW, and BOH exposed to carbonate (k-range: 3-12.5 $Å^{-1}$; R-range: 1.2-4.158 Å; $S_0^2 = 0.85$; $E_0 = 13422$ eV)

Sample	Path	Coordination Number, CN	Bond Distance, R (Å)	Sigma Squared, σ^2 ($Å^2$)	ΔE_0 (eV)	Chi_r^2	R-factor
BOH + DIW	Bi-O Bi-O Bi-O Bi-Bi	2.0 ± 0.2 1.1 ± 0.2 0.7 ± 0.2 8.2 ± 3.8	2.12 (1) 2.63 (2) 2.95 (4) 3.64 (3)	0.006 (1) 0.006 (1) 0.006 (1) 0.024 (5)	-10 ± 1.5	19.0	0.01
BOH + carbonate	Bi-O Bi-C Bi-Bi	0.8 ± 0.1 1.9 ± 0.9 4.3 ± 1.4	2.24 (1) 3.42 (3) 3.72 (2)	0.008 (2) 0.013 (7) 0.022 (3)	-4.6 ± 1.5	18.9	0.03

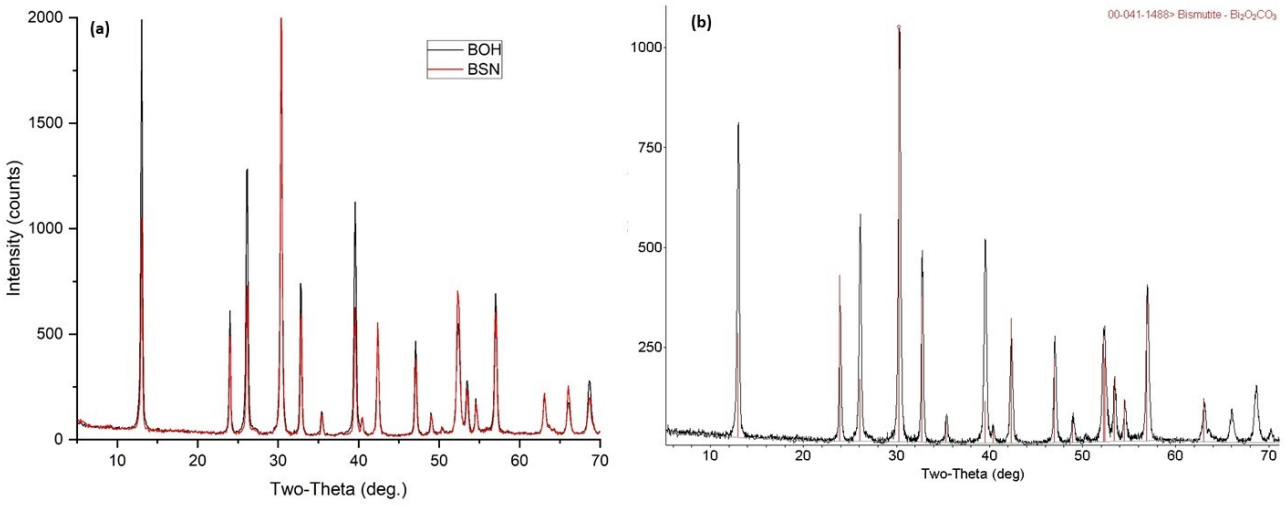

Figure S4: XRD patterns for BOH and BSN after exposure to carbonate (a) with corresponding pattern for bismutite (b).

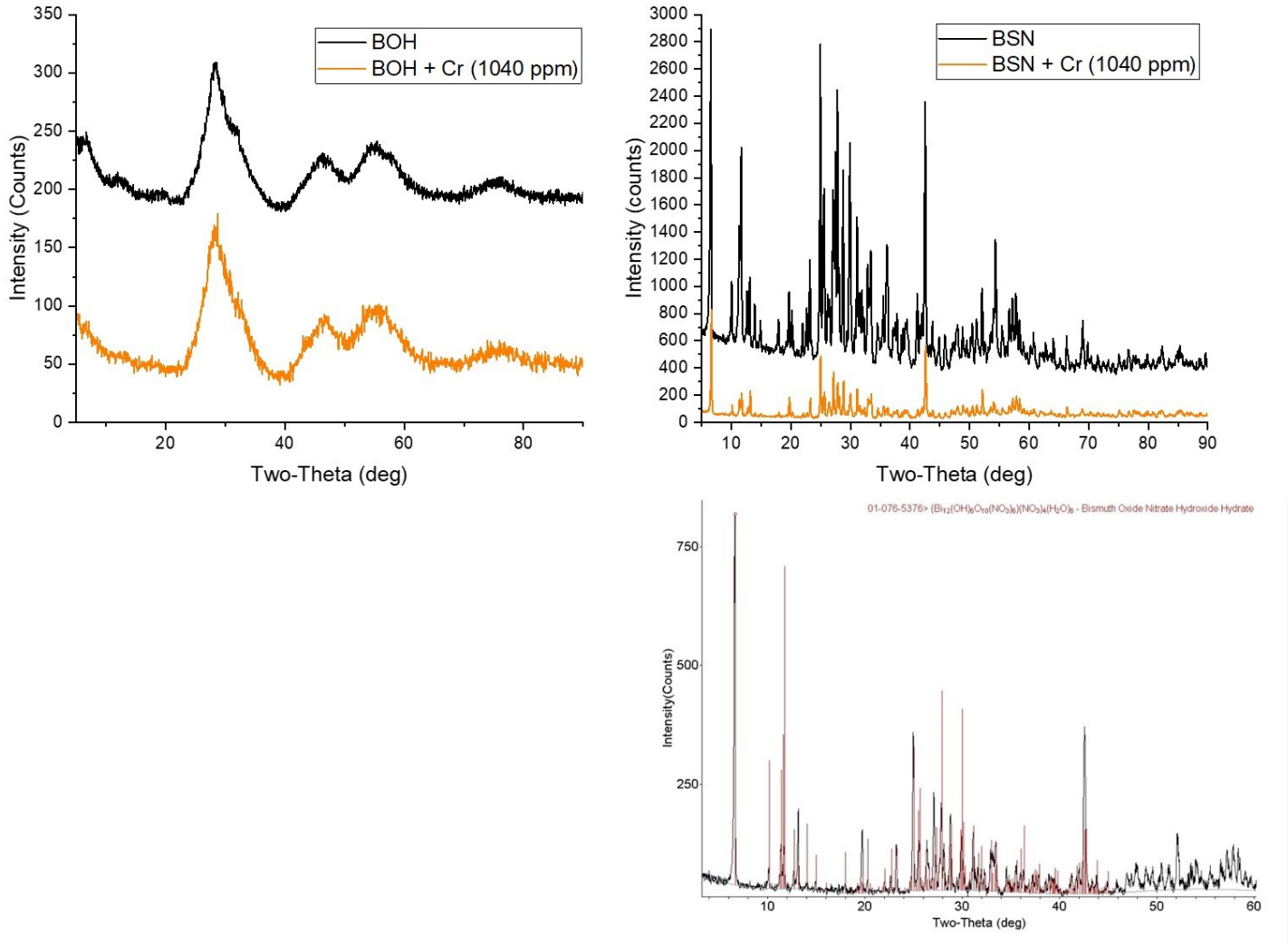

Figure S5: XRD pattern for BOH before (black) and after (yellow) exposure to 1040 ppm Cr (sample S), and for BSN before (black) and after (yellow) exposure to 1040 ppm Cr (top) and match for BSN contacted with 1040 ppm Cr for 24 hours to *clus*-$Bi_{12}O_{10}(OH)_6(NO_3)_{10}\cdot 6(H_2O)$ (bottom).

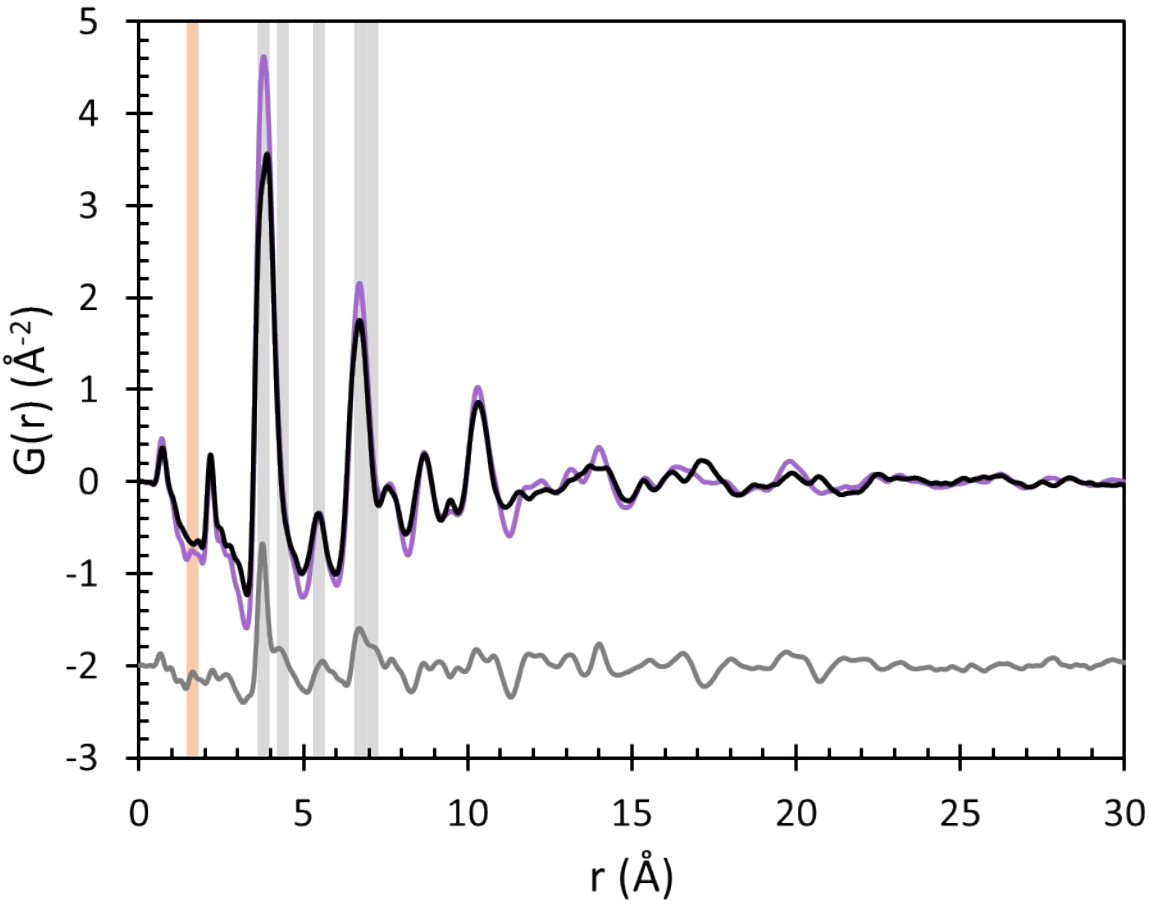

Figure S6: XPDF profile of Cr-reacted BOH (purple) in comparison with the as-synthesized BOH material (black). The differential XPDF is shown in grey, offset by 2 $Å^{-2}$. Bismutite structural features are highlighted by the light grey bands. The Cr-O distance at 1.64 Å is highlighted in light orange.

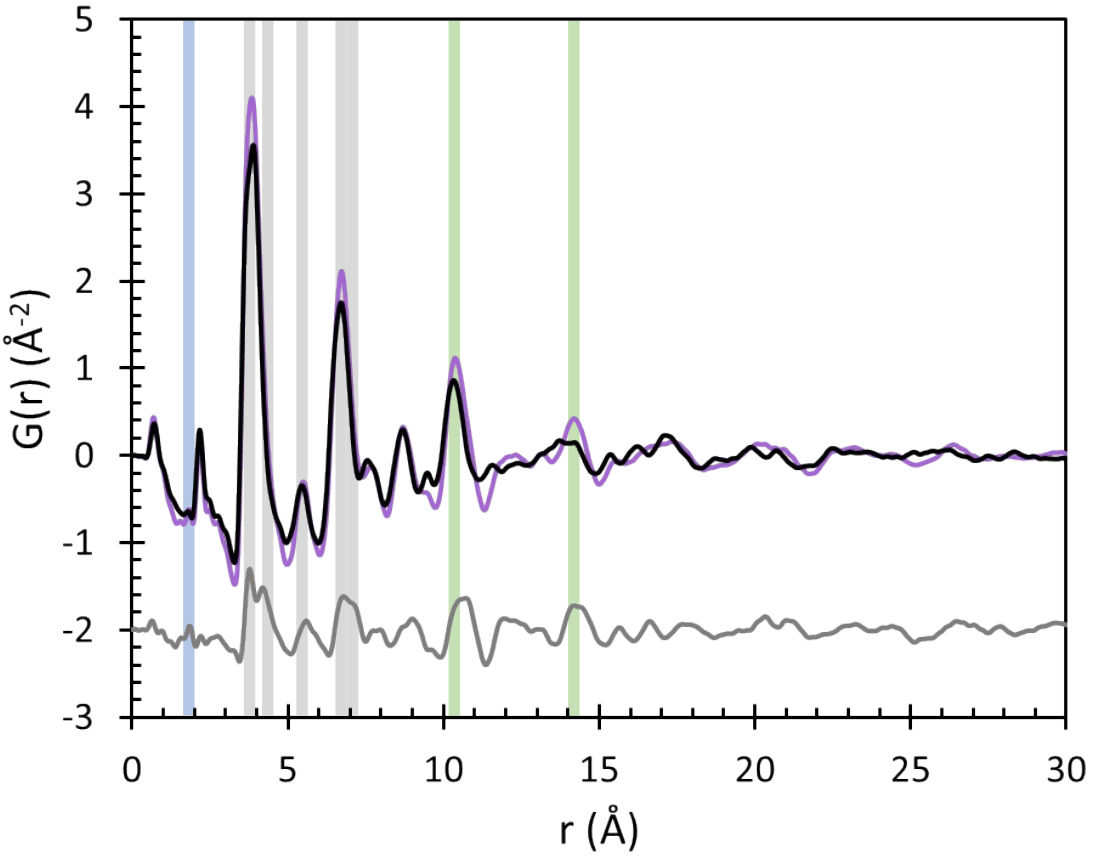

Figure S7. XPDF profile of I-reacted BOH (purple) in comparison with the as-synthesized material (black). The differential XPDF is shown in grey, offset by 2 $Å^{-2}$. Bismutite structural features are highlighted by the light grey bands. The distance at 1.92 Å is highlighted in light blue. Additional medium- to longer-range features are highlighted in light green.

Table S2: ICP-OES Cr results for BOH and BSN exposed to high concentrations of Cr (~1000 mg/L) in the presence of either Hanford SGW or DIW.

Test Name	Matrix	pH	ICP-OES	Cr (mg/L)	EQL (mg/L)
Cr-BOH-1	Hanford SGW	**7.825**	√	ND	0.256
Cr -BOH-2	Hanford SGW	**8.067**	√	ND	0.256
Cr -BOH-3	Hanford SGW	**7.410**	√	ND	0.256
Cr-BSN-1	Hanford SGW	**7.234**	√	779	0.256
Cr-BSN-2	Hanford SGW	**7.198**	√	792	0.256
Cr-BSN-3	Hanford SGW	**7.251**	√	781	0.256
Cr -Blk-SGW	Hanford SGW	**8.285**	√	1030	0.256
Cr-BOH-4	DIW	**7.358**	√	ND	0.256
Cr -BOH-5	DIW	**6.852**	√	ND	0.256
Cr -BOH-6	DIW	**6.706**	√	ND	0.256
Cr-BSN-4	DIW	**7.092**	√	800	0.256
Cr-BSN-5	DIW	**7.052**	√	811	0.256
Cr-BSN-6	DIW	**7.057**	√	780	0.256
Cr -Blk-DDI	DIW	**8.010**	√	1040	0.256

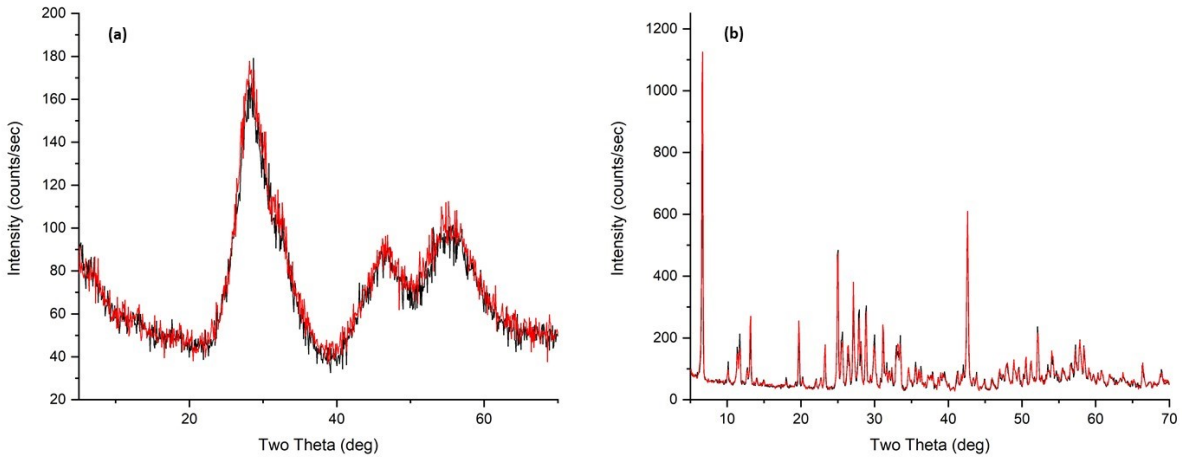

Figure S8: XRD patterns for (a) BOH and (b) BSN after exposure to 1040 ppm Cr in DIW (red) or 1040 ppm Cr in Hanford SGW (black).

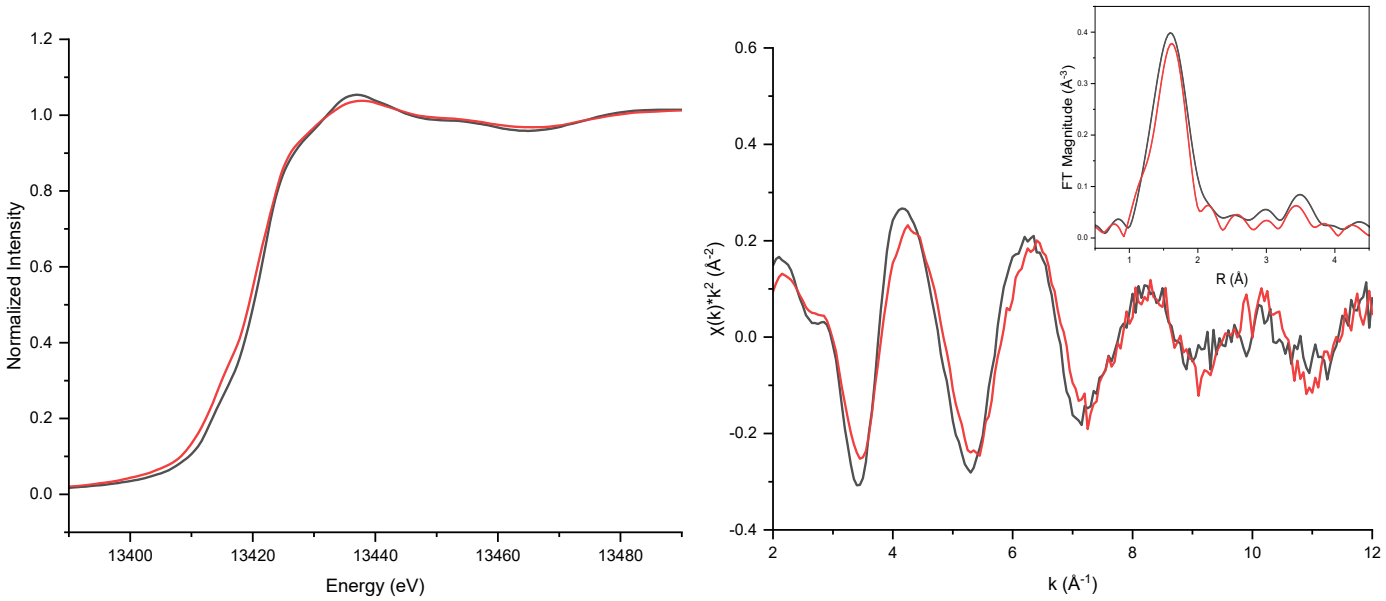

Figure S9: Bi L_{III}-edge XANES spectra; k^2-weighted $\chi(k)$ spectra and Fourier transform magnitude for BOH in water (black line) and Cr associated BOH (red line).

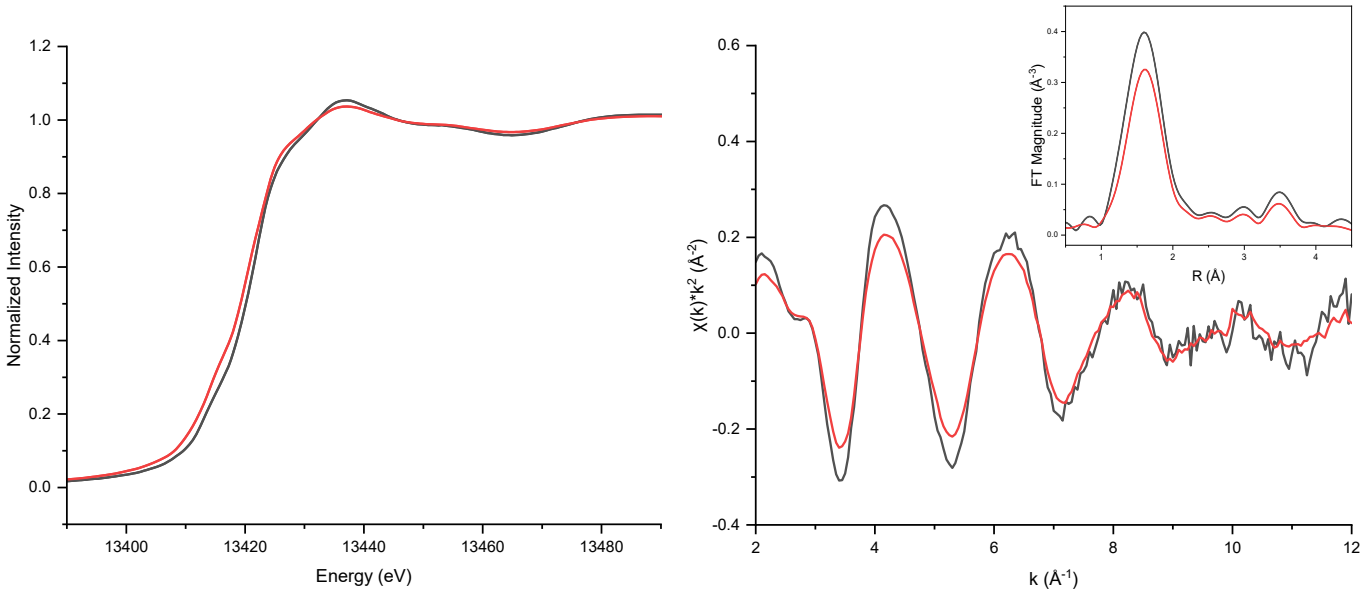

Figure S10: Bi L_{III}-edge XANES spectra; k^2-weighted χ(k) spectra and Fourier transform magnitude for BOH in water (black line) and I associated BOH (red line).

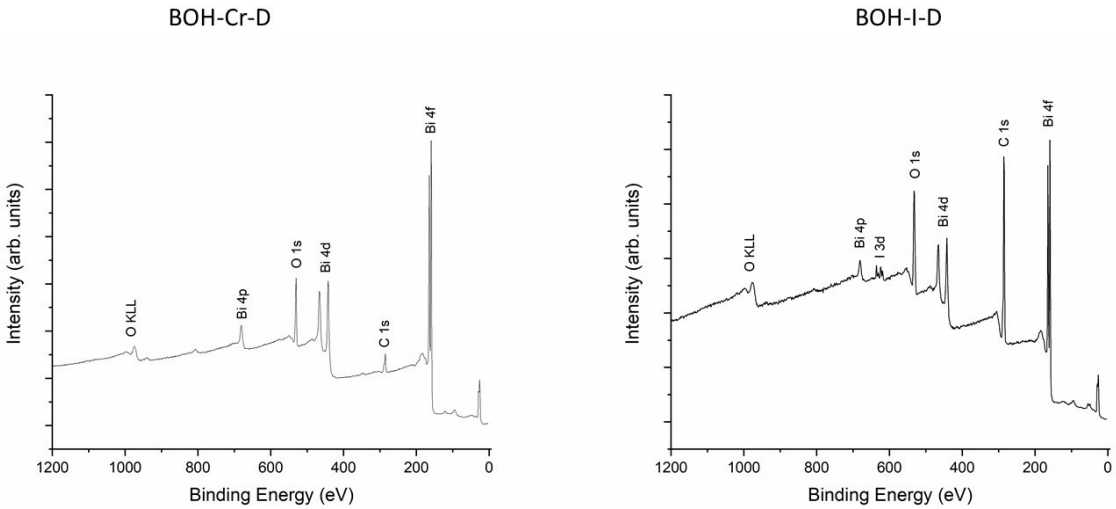

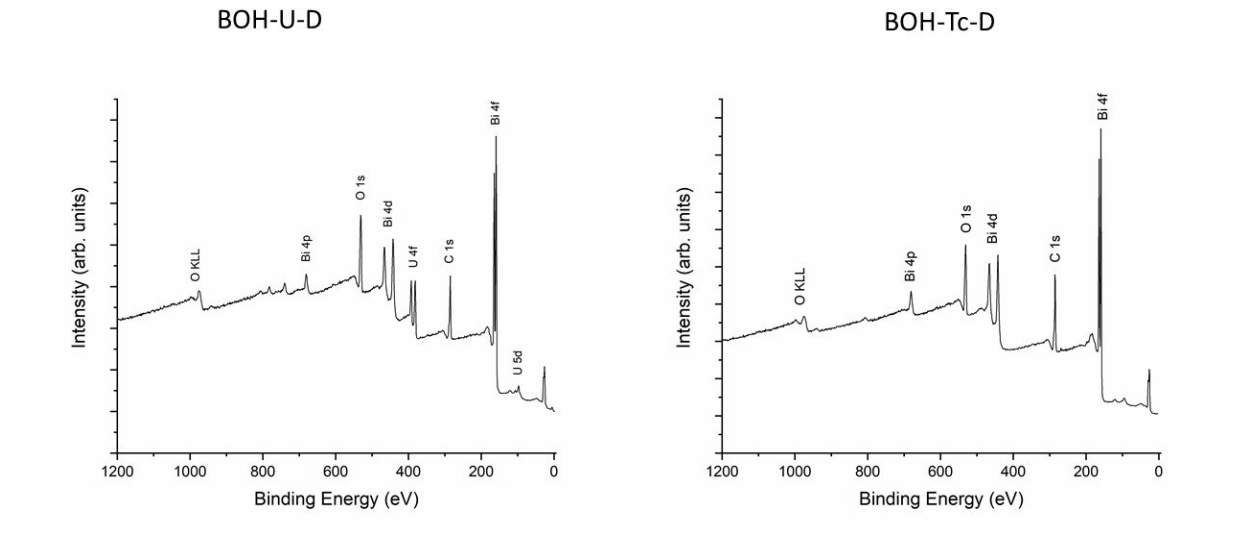

Figure S11. XPS survey scans for BOH after exposure to approximately $1 \cdot 10^{-4}$ M of Cr, U, Tc (sample D) and $1.5 \cdot 10^{-3}$ M of I (sample E).

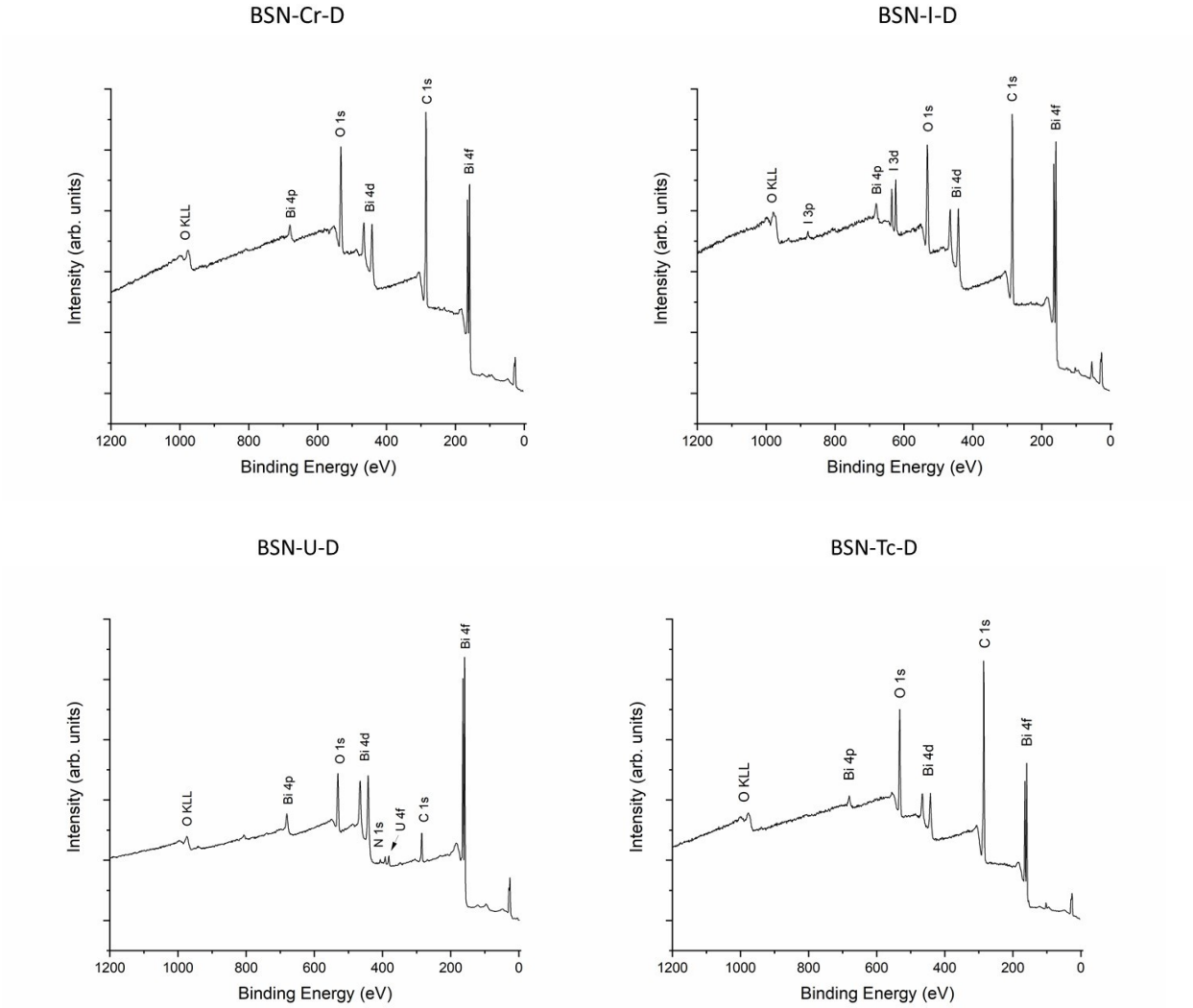

Figure S12. XPS survey scans for BSN after exposure to approximately $1 \cdot 10^{-4}$ M of Cr, U, Tc (sample D) and $1.5 \cdot 10^{-3}$ M of I (sample E).

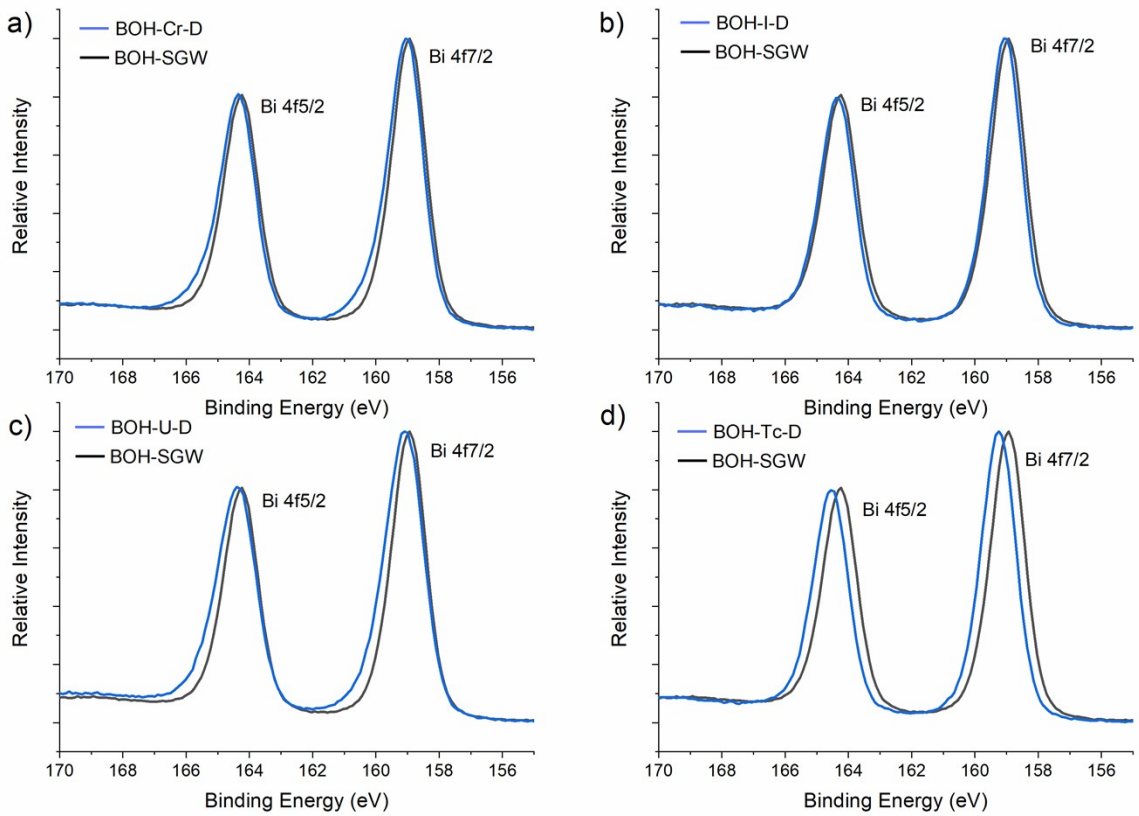

Figure S13. Bi 4f5/2 XPS spectra for BOH after exposure to Hanford SGW and approximately $1 \cdot 10^{-4}$ M of Cr, U, Tc (sample D) and $1.5 \cdot 10^{-3}$ M of I (sample E).

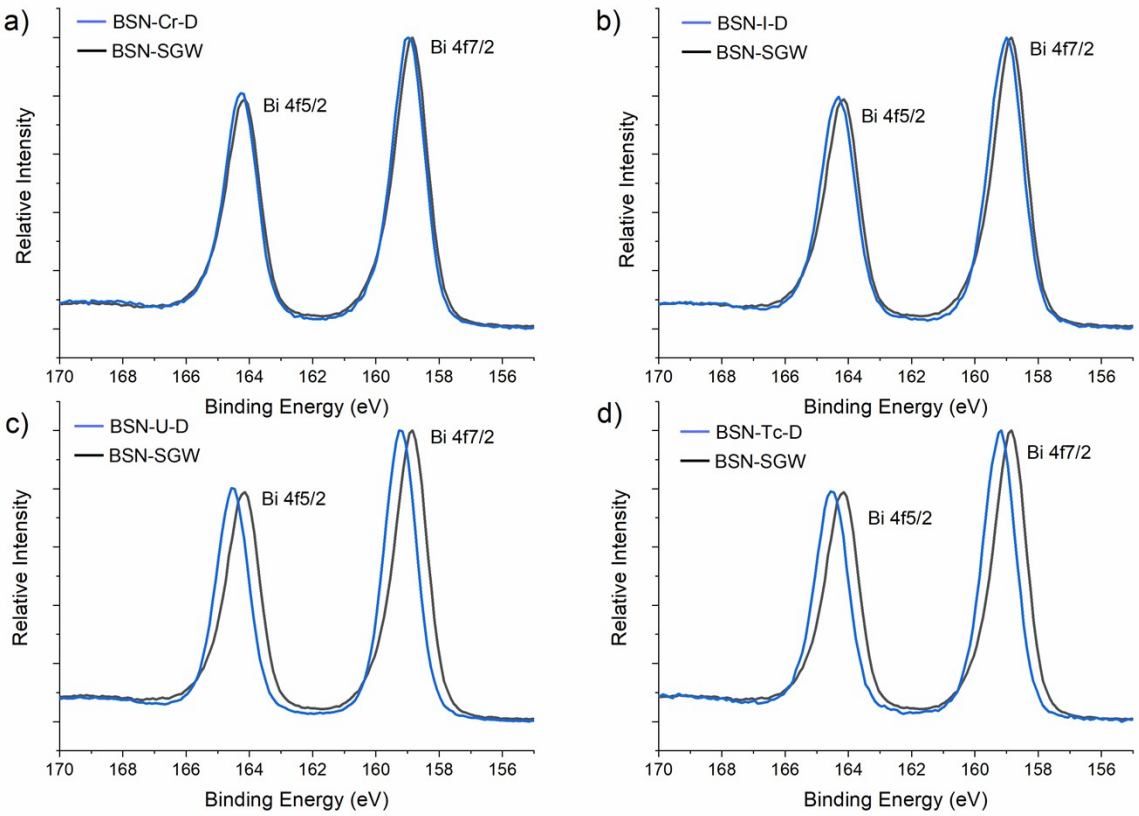

Figure S14. Bi 4f5/2 XPS spectra for BSN after exposure to Hanford SGW approximately $1.7 \cdot 10^{-4}$ M of Cr, U, Tc (sample D) and $1.5 \cdot 10^{-3}$ M of I (sample E).

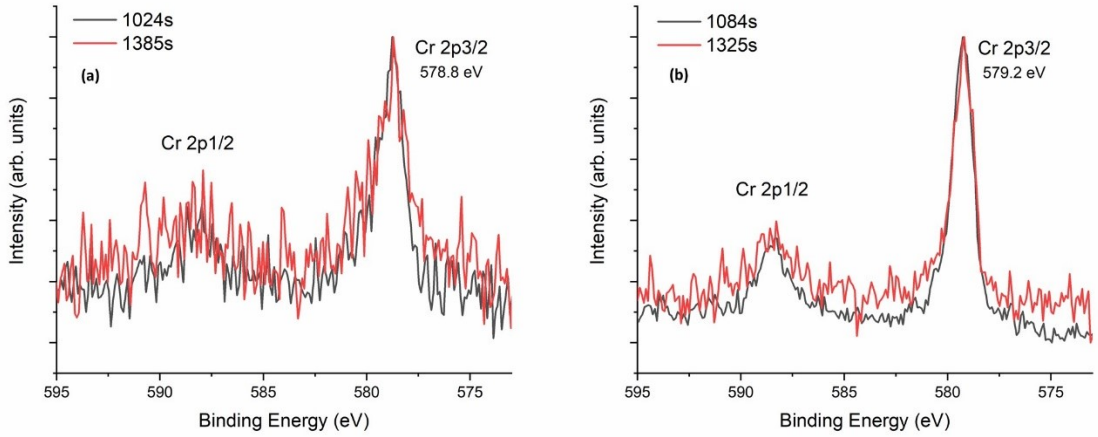

Figure S15. Cr 2p XPS spectra collected for different lengths of time for (a) BOH exposed to 1040 ppm Cr and (b) BSN exposed to 1040 ppm Cr (sample S).

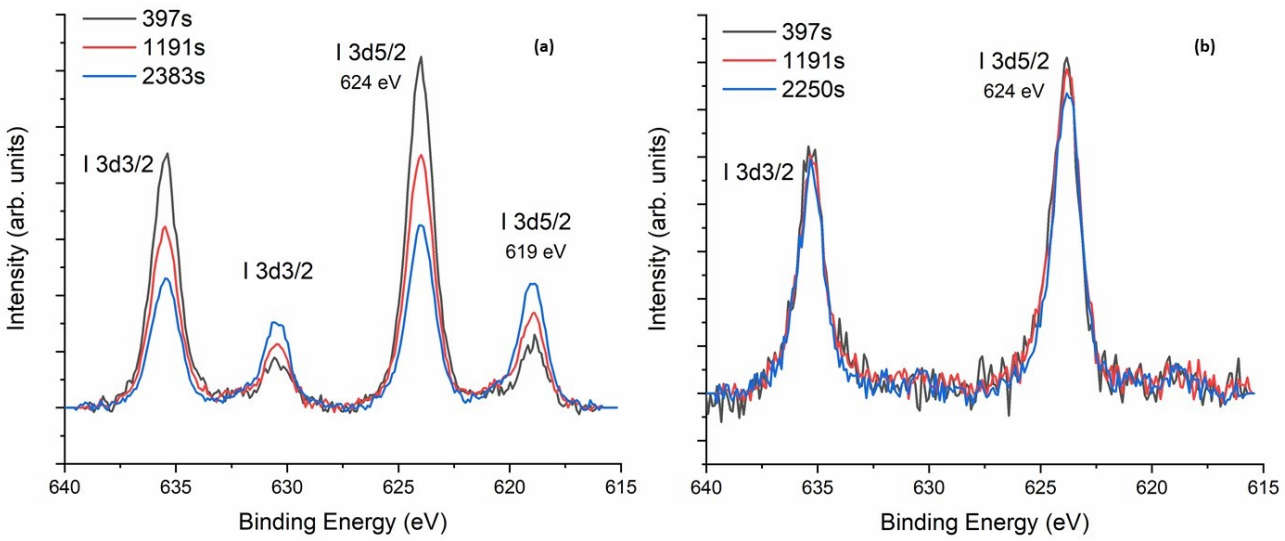

Figure S16. I 3d XPS spectra collected for different lengths of time for (a) BOH exposed to 190 ppm I and (b) BSN exposed to 190 ppm I.

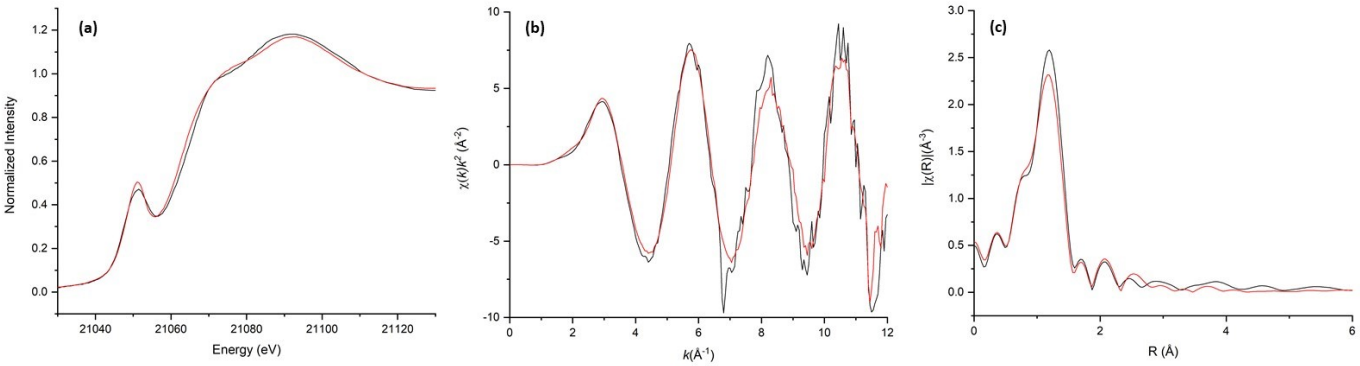

Figure S17: (a) Tc K-edge XANES spectra; (b) k^2-weighted χ(k) spectra; (c) Fourier transform (FT) magnitude for Tc associated with BOH (black line) and for NH_4TcO_4 (red line).

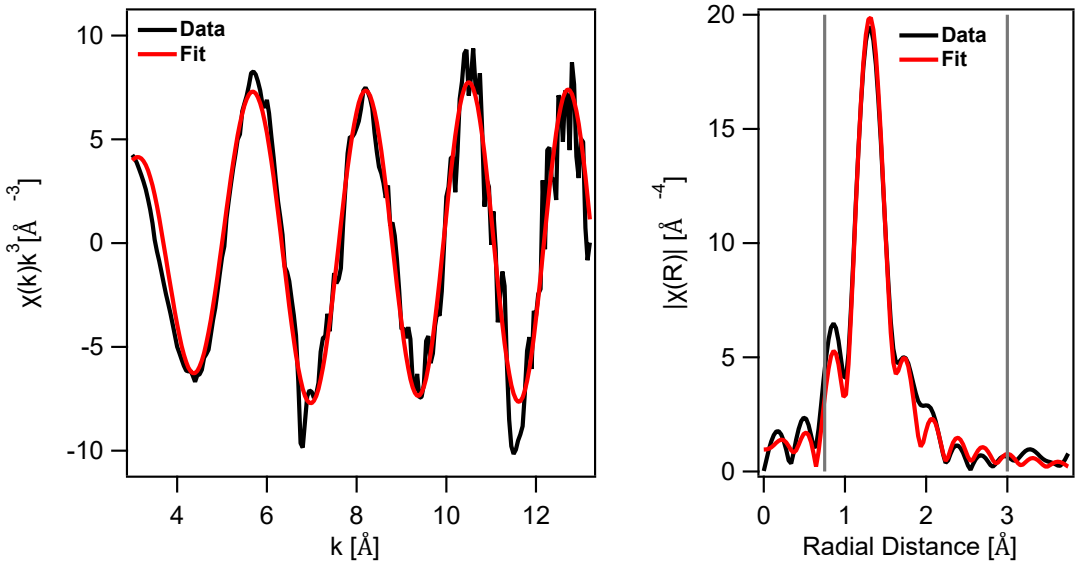

Figure S18: EXAFS spectrum (black) and fit (red) (left panel) and its Fourier transform (right panel). Grey

lines indicate the Fourier transform fit window.

Table S3: Fitting parameters[a]

Neighbor	CN	Distance (Å)	σ^2 (Å^2)	Reff
O	4[b]	1.735 (4)	0.0001(2)	4 O at 1.737 Å[c]

a) S_0^2= 0.95 (fixed), ΔE= -3(1) eV;
b) Fixed Value
c) Weaver et al., 2017.

XPS analysis: U 4f XPS Fitting Parameters

A Shirley background was applied to the U 4f region starting at about 5 eV below the U 4f7/2 peak and extending beyond 15 eV of the U 4f5/2 peak. The peaks were fitted using Gaussian-Lorentzian type components [GL(65)] in CasaXPS. The fitting parameters for each component are given in Tables S5 and S6. The satellite intensities found at 4 eV and 10 eV are characteristic for U(VI) systems. The component with U 4f7/2 BE of 380.2 eV was assigned to a U(V) species. Although this binding energy is close to a U(IV) species, the satellite peak at about 8.19 eV above the main peak is well within the range of reported values for U(V) compounds. Moreover, beam-induced reduction of U(VI) to U(V) is also quite well known in literature (Ilton et al., 2007).

Table S4: U 4f XPS fitting parameters used for BOH-U-D. Position, intensity, FWHM values reported are relative to the corresponding main peaks. A GL(65) peak shape has been used for all peaks.

U(VI)			**U(V)**		
Primary Peaks			**Primary Peaks**		
Position of U 4f7/2 (eV)	381.7		Position of U 4f7/2 (eV)	380.2	
Spin orbit splitting (eV)	10.8		Spin orbit splitting (eV)	10.76	
Branching ratio (5/2:7/2)	0.75		Branching ratio (5/2:7/2)	0.73	
FWHM	1.7		FWHM	1.3	
Satellites			**Satellites**		
	U 4f7/2	**U 4f5/2**		**U 4f7/2**	**U 4f5/2**
Position (eV)	+1.78	+1.78	Position (eV)	+8.19	+8.19
Intensity (eV)	x 0.077	x 0.077	Intensity (eV)	x 0.097	x 0.097
FWHM	x 1	x 1	FWHM	x 1.16	x 1.16
Position (eV)	+3.77	+3.77			
Intensity (eV)	x 0.072	x 0.072			
FWHM	x 1.14	x 1.14			
Position (eV)	+10.1	+10.1			
Intensity (eV)	x 0.05	x 0.05			
FWHM	x 1.47	x 1.47			

Table S5: U 4f XPS fitting parameters used for BSN-U-D. Position, intensity, FWHM values reported are relative to the corresponding main peaks. A GL(65) peak shape has been used for all peaks.

U(VI)		
Primary Peaks		
Position of U 4f7/2 (eV)	381.6	
Spin orbit splitting (eV)	10.8	
Branching ratio (5/2:7/2)	0.72	
FWHM	1.44	
Satellites		
	U 4f7/2	**U 4f5/2**
Position (eV)	+1.45	+1.45
Intensity (eV)	x 0.1	x 0.1
FWHM	x 1.5	x 1.5
Position (eV)	+3.4	+3.4
Intensity (eV)	x 0.09	x 0.09
FWHM	x 1.7	x 1.7
Position (eV)	+10.0	+10.0
Intensity (eV)	x 0.09	x 0.09
FWHM	x 1.7	x 1.7

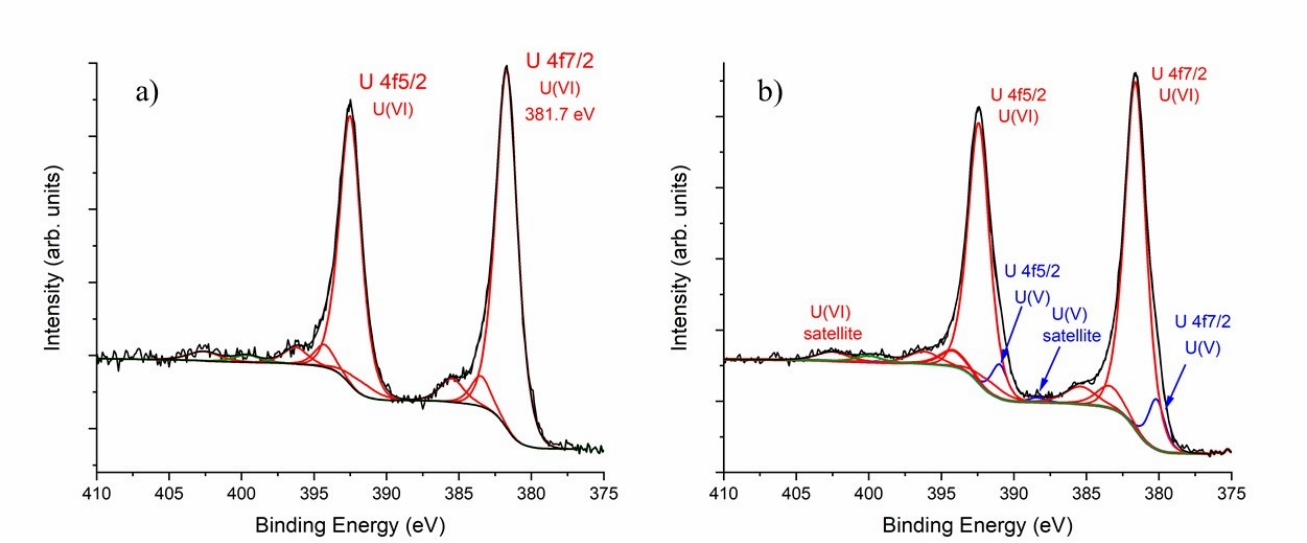

Figure S19. Peak-fitted U 4f XPS spectra showing X-ray beam induced reduction of U(VI) on BOH-U-D. a) Spectra obtained for a scan time of 457s. b) Spectra acquired for a total scan time of 2895s. The feature at 399.7 eV (in green) is assumed to be a reduced nitrogen species.

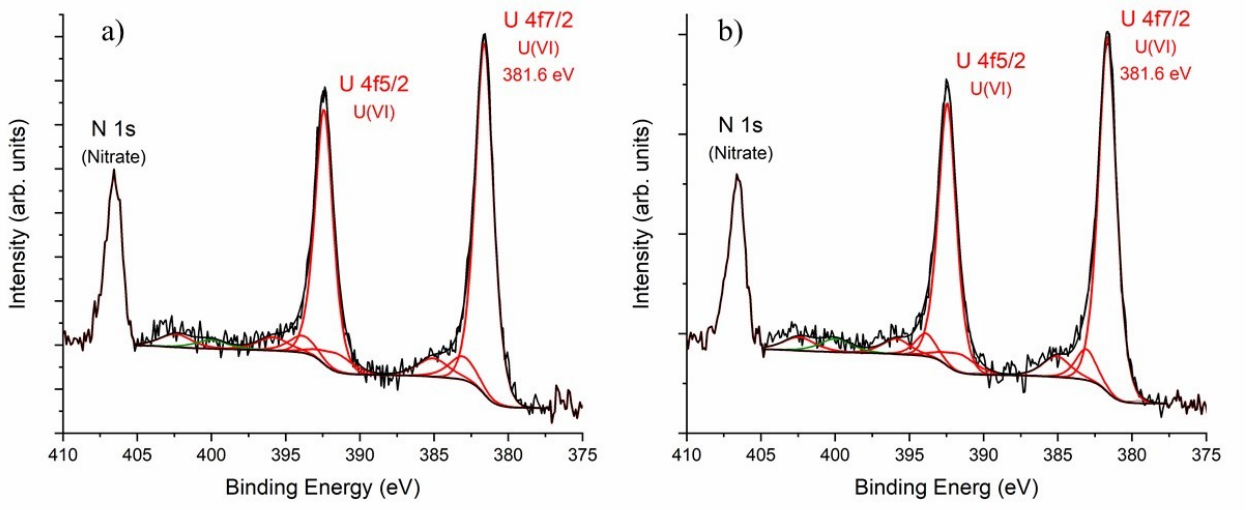

Figure S20. Peak-fitted U 4f XPS spectra showing no X-ray beam induced reduction in BSN-U-D. a) Spectra obtained for a scan time of 1347s. b) Spectra acquired for a total scan time of 3031s. The feature at 399.7 eV (in green) is assumed to be a reduced nitrogen species.

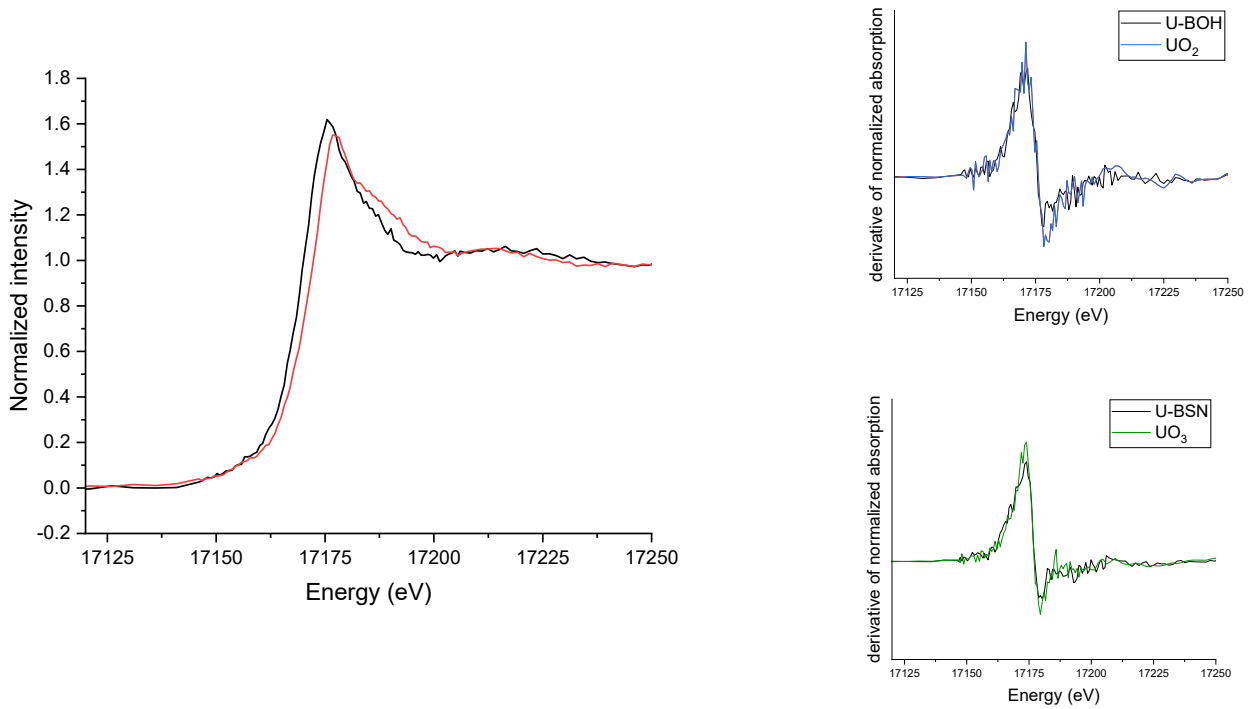

Figure S21. U L_{III}-edge XANES spectra for U associated with BOH (black) and BSN (red) materials and their corresponding derivatives compared to U(IV) and U(VI) oxides.

References

Ilton, E. S., Boily, J.-F. and Bagus, P. S. (2007). Beam induced reduction of U(VI) during X-ray photoelectron spectroscopy: The utility of the U4f satellite structure for identifying uranium oxidation states in mixed valence uranium oxides, *Surface Science 601*, 908–916.

Lazarini, F. (1978). The crystal structure of a bismuth basic nitrate, $[Bi_6O_5(OH)_3](NO_3)_5 \cdot 3\ H_2O$. *Acta Crystallographica Section B: Structural Crystallography and Crystal Chemistry*, *34*(11), pp.3169-3173

Weaver, J., Soderquist, C. Z., Washton, N. M., Lipton, A. S., Gassman, P. L., Lukens, W. W., Kruger, A. A., Wall, N. A. and McCloy, J. S. (2017). Chemical Trends in Solid Alkali Pertechnetates. *Inorganic Chemistry 56*, 2533.

Zhen Li; Guorui Feng; Yi Luo; Shengyong Hu; Tingye Qi; Haina Jiang; Jun Guo; Jinwen Bai; Xianjie Du; Lixun Kang; AIP Advances 7, 085204 (2017) DOI: 10.1063/1.4997749